axioms

MDPI

Article

Observer-Linked Branching (OLB)—A Proposed Quantum-Theoretic Framework for Macroscopic Reality Selection

Călin Gheorghe Buzea [1,*], Florin Nedeff [2,*], Valentin Nedeff [2], Dragos-Ioan Rusu [2], Maricel Agop [3] and Decebal Vasincu [4]

[1] National Institute of Research and Development for Technical Physics, IFT Iași, 700050 Iași, Romania
[2] Department of Environmental Engineering, Mechanical Engineering and Agritourism, Faculty of Engineering, "Vasile Alecsandri" University of Bacău, 600115 Bacău, Romania; vnedeff@ub.ro (V.N.); drusu@ub.ro (D.-I.R.)
[3] Physics Department, "Gheorghe Asachi" Technical University Iași, 700050 Iași, Romania; m.agop@yahoo.com
[4] Department of Emergency Medicine, "Grigore T. Popa" University of Medicine and Pharmacy, 700115 Iasi, Romania; decebal.vasincu@umfiasi.ro
* Correspondence: calinb2003@yahoo.com (C.G.B.); florin_nedeff@ub.ro (F.N.)

Abstract

We propose Observer-Linked Branching (OLB), a mathematically rigorous extension of quantum theory in which an observer's cognitive commitment actively modulates collapse dynamics at macroscopic scales. The OLB framework rests on four axioms, employing a norm-preserving nonlinear Schrödinger evolution and Lüders-type projection triggered by crossing a cognitive commitment threshold. Our expanded formalism provides five main contributions: (1) deriving Lie symmetries of the observer–environment interaction Hamiltonian; (2) embedding OLB into the Consistent Histories and path-integral formalisms; (3) multi-agent network simulations demonstrating intentional synchronisation toward shared macroscopic outcomes; (4) detailed statistical power analyses predicting measurable biases (up to ~5%) in practical experiments involving traffic delays, quantum random number generators, and financial market sentiment; and (5) examining the conceptual, ethical, and neuromorphic implications of intent-driven reality selection. Full reproducibility is ensured via the provided code notebooks and raw data tables in the appendices. While the theoretical predictions are precisely formulated, empirical validation is ongoing, and no definitive field results are claimed at this stage. OLB thus offers a rigorous, norm-preserving and falsifiable framework to empirically test whether cognitive engagement modulates macroscopic quantum outcomes in ways consistent with—but extending—standard quantum predictions.

Keywords: observer-dependent quantum mechanics; macroscopic superposition; collapse dynamics; intentionality in physics; quantum measurement problem

MSC: 81P15

check for updates

Academic Editors: Oscar Montiel Ross and João Nuno Prata

Received: 20 May 2025
Revised: 1 July 2025
Accepted: 2 July 2025
Published: 8 July 2025

Citation: Buzea, C.G.; Nedeff, F.; Nedeff, V.; Rusu, D.-I.; Agop, M.; Vasincu, D. Observer-Linked Branching (OLB)—A Proposed Quantum-Theoretic Framework for Macroscopic Reality Selection. *Axioms* **2025**, *14*, 522. https://doi.org/10.3390/axioms14070522

Copyright: © 2025 by the authors. Licensee MDPI, Basel, Switzerland. This article is an open access article distributed under the terms and conditions of the Creative Commons Attribution (CC BY) license (https://creativecommons.org/licenses/by/4.0/).

1. Introduction

The standard formulation of quantum mechanics permits the linear superposition of mutually incompatible states, yet our macroscopic experience remains singular and determinate. This contrast—between the superpositional ontology of the microscopic world and the definiteness of classical measurement outcomes—constitutes the measurement problem, one of the most enduring conceptual puzzles in physics.

Several interpretative and dynamical extensions of quantum theory have been proposed to address this discrepancy. Decoherence theory, by showing how entanglement with an environment rapidly suppresses interference terms in a reduced density matrix, explains the appearance of classicality [1]. Decoherence alone, however, does not select which outcome actually occurs. To fill that explanatory gap, a variety of frameworks have emerged. Relational Quantum Mechanics (RQM) views the wave function as a catalogue of relations rather than absolute states [2]; QBism interprets collapse as a Bayesian update by an individual agent [3]; and Wheeler's participatory realism and related Wigner- and Pauli-type proposals argue that observational acts, possibly involving consciousness, bring physical reality into being [4,5]. Objective-collapse models—the GRW theory, the Diósi–Penrose mechanism and their variants—insert spontaneous stochastic localisation terms that act independently of observers [6–8]. Finally, the consistent-histories programme provides a decoherent ontology of mutually exclusive classical histories with well-defined probabilities but no single preferred realisation [9]. Each of these theories offers a partial resolution, yet none explicitly incorporates an observer's decisional structure as a bona fide dynamical variable, nor do they specify how commitment to a single alternative modulates branching weights in real time.

The Observer-Linked Branching (OLB) framework is designed to close that gap. It postulates that cognitive commitment functions as a physical trigger for branch selection without violating the core quantum formalism or invoking hidden ontic variables. Specifically, OLB assumes that an observer's internal state evolves continuously inside a dedicated Hilbert space $\mathcal{H}_O$; that the observer's trajectory $\gamma_O(t)$ through this space continuously modulates a bias channel shaping environmental branch weights; and that collapse occurs—neither randomly nor spontaneously—when a measurable commitment threshold is reached, a threshold tied to physiological signatures that can in principle be recorded.

Unlike metaphysical theories of mind, OLB treats commitment as a neuro-cognitive process, potentially detectable via behavioural or electrophysiological markers. The central question therefore becomes: can this process influence branching probabilities in a manner consistent with quantum structure yet not reducible to it?

Empirical antecedents. A small but steadily expanding experimental literature already probes whether focused intention can bias nominally random physical processes. Early mind–machine-interaction studies at the Princeton Engineering Anomalies Research (PEAR) laboratory reported millideviation-level shifts in diode-based random generators when operators strove for high or low counts; a 380-series meta-analysis covering 35 years of data yielded an overall effect size of about 10^{-4} with a Stouffer $Z = 6.4$ ($p \approx 10^{-10}$) [10,11]. More recently, Radin et al. employed a double-slit interferometer and found that periods of sustained human attention reduced single-photon fringe visibility by roughly 6 % relative to matched no-observer blocks, with a Bayes factor exceeding 150 in favour of an attention effect [12]. Complementary neurophysiological work shows that the P300/CPP complex—a centro-parietal positivity that peaks about 300 ms after evidence accumulation reaches a decision bound—is a robust neural signature of commitment; its amplitude correlates with subjective certainty and with downstream motor-execution latency [13,14]. Because both the PEAR meta-analysis and the double-slit attention study remain subjects of active debate, they are cited here only as motivating anomalies; the burden of decisive verification is carried by the prospective protocols outlined later in this paper. Together, these studies provide a measurable threshold signal of precisely the kind posited in OLB.

Macroscopic echoes. Field observations mirror these laboratory hints. Helbing's analysis of highway traffic demonstrates that densely connected driver cohorts anticipating congestion generate stop-and-go waves significantly earlier than car-following models lacking a shared anticipatory state can reproduce [15,16]. Similarly, dense-audience experi-

ments reveal that bursts of perfectly synchronised clapping erupt in a two-thousand-seat auditorium with a frequency that exceeds Poisson expectations by an order of magnitude; statistical modelling shows that such bursts cannot be explained without introducing a latent "shared-intention" variable [17,18]. Although each phenomenon admits classical alternative explanations, taken together they motivate a testable hypothesis: decisional commitment—indexed by neuro-cognitive thresholds—may act as an effective control parameter on branch probabilities even in mesoscopic systems. OLB translates that qualitative suggestion into a quantitative framework.

Such effects are often dismissed as experimental artefacts or cognitive bias. OLB proposes instead that they may reflect genuine deviations from purely random branching modulated by coordinated internal states.

Key contributions of OLB. The present work therefore contributes (i) a dynamical model of measurement in which observer commitment behaves as a physical field; (ii) a testable hypothesis linking intention-driven bias to measurable shifts in branching outcomes; (iii) a mathematical structure that embeds seamlessly inside orthodox quantum mechanics—unitary evolution, Lüders projection and consistent histories; and (iv) a suite of realistic simulations and experimental proposals, ranging from traffic flow to photon-based random-number generators and financial markets, that can put the predictions of OLB to empirical test.

Although the historical dialogue between Pauli and Jung foreshadowed a participatory stance, the present model is grounded instead in contemporary quantum foundations and empirical data. In cognitive science, Hilbert-space models capture violations of classical probability axioms, order effects in decision-making, and superposition-like belief states [19–21]. In the social sciences, they describe non-classical correlations in market behaviour, trust dynamics and multi-agent synchronisation [22]. These models do not imply that neurons or societies obey microscopic quantum laws; rather, they show that quantum mathematics supplies a tractable language for systems possessing epistemic uncertainty and dynamic entanglement between observer and environment. In this spirit, OLB treats the cognitive trajectory $\gamma_O(t)$ and commitment threshold θ not as metaphysical abstractions but as variables that can be measured and manipulated experimentally. The empirical aim is not to declare "consciousness collapses the wavefunction" but to determine whether intentional engagement measurably alters branching statistics in ways that surpass classical randomness and are predictable by an extended decoherence framework.

Broader perspective and paper outline. If the holographic principle holds—that is, if the universe's information content is fundamentally encoded on lower-dimensional boundaries—then the apparent separation between microscopic quantum behaviour and macroscopic classicality may reflect a difference of scale rather than of kind. In that view, the mathematical structures that govern particles and fields—superposition, contextuality and projection—could also emerge in systems with very high information density, such as cognition, collective decision-making or large-scale coordination.

Although OLB does not require a holographic ontology, it resonates with this broader intuition: quantum-like principles can manifest outside the microphysical domain whenever information flow, internal dynamics and agency are central. The aim is not to erase disciplinary boundaries, but to test—in a controlled and falsifiable way—whether the tools of quantum theory continue to hold in mesoscopic and macroscopic regimes.

While the conceptual foundation of OLB may appear speculative at first glance, our aim is not to propose metaphysical claims but to formulate empirically testable predictions derived from a well-defined mathematical structure. The framework adheres to standard quantum principles—unitarity, Lüders projection, and no-signalling—and incorporates measurable neurophysiological signals (e.g., commitment thresholds) as parameters. Al-

though the coupling of cognitive commitment to collapse dynamics extends traditional quantum models, it does so within a falsifiable and data-driven paradigm. This ensures that OLB remains within the bounds of rigorous scientific inquiry.

This paper develops the theoretical and empirical foundations of OLB. Section 2 introduces the core mathematical structure: the observer–environment Hilbert space, the bias-modulated interaction Hamiltonian, and the collapse criterion tied to commitment. Section 3 presents simplified simulations that illustrate the consequences of cognitive bias in branching outcomes. Section 4 proposes empirical protocols—across traffic systems, quantum RNGs, and market dynamics—to test OLB predictions. Section 5 situates the model within existing interpretations, highlighting compatibilities and differences. Section 6 addresses open problems, including relativistic covariance, thermodynamic cost, and neurophysiological correlates of commitment. Section 7 reflects on ethical implications, and Section 8 outlines next steps.

2. Formal Framework of Observer-Linked Branching (OLB)

To develop a testable theory of observer-influenced collapse, we introduce a formalism that embeds cognitive commitment into quantum dynamics using a minimal set of extensions. The approach is grounded in four axioms and uses standard quantum structures—Hilbert spaces, Hermitian operators, and Lüders projection—but applies them to a coupled observer–environment system in which the observer's internal state actively shapes collapse dynamics.

System Overview

We model the total system as a tensor product of two Hilbert spaces:

- $\mathcal{H}_E$ (Environmental space): Represents macroscopically distinguishable alternatives—e.g., traffic conditions, detector outcomes, or market states. It is spanned by an orthonormal basis $\{|e_i\rangle\}_{i=0}^{N-1}$, where N is the number of branches resulting from environmental decoherence.
- $\mathcal{H}_O$ (Observer space): A finite-dimensional Hilbert space representing internal cognitive modes of the observer. We define a preferred orthonormal basis $\{|o_j\rangle\}$, with $o_j \in$ {passive, watching, acting, committed}, to describe functional cognitive states.
- $\mathcal{H} = \mathcal{H}_E \otimes \mathcal{H}_O$: The full ontic space of the observer-environment system. All evolution occurs in this joint space.

Key Dynamical Elements

- $\gamma_O(t) \in \mathcal{H}_O$: The observer's internal state trajectory. It evolves continuously in time and reflects moment-to-moment changes in cognitive mode (e.g., shifting from observation to commitment). This internal trajectory acts as a control parameter for environmental coupling.
- $g_i(\gamma_O(t)) \in$ R: A bias function—real, bounded, and Lipschitz-continuous—assigned to each branch e_i. It quantifies how compatible the observer's internal state is with that branch at time t. These functions distort otherwise neutral quantum probabilities, allowing the observer's readiness to commit to shape-collapse likelihood.
- $P_{comm} = |commited\rangle\langle commited| \otimes 1_E$: A projector onto the committed cognitive state in $\mathcal{H}_O$, tensor the identity on the environment. This operator is used to define the collapse condition.
- $N \in \mathbb{N}$: The number of decohered macroscopic alternatives in the environment. This determines the dimensionality of $\mathcal{H}_E$.

Time-Dependent Interaction Hamiltonian

With these components in place, we define the interaction Hamiltonian that governs the modulation of environmental weights by the observer:

$$H_{int}(t) = \sum_{i=0}^{N-1} g_i(\gamma_O(t)) |e_i\rangle \langle e_i| \bigotimes P_{comm} \quad (1)$$

This term describes how the environmental branch weights become distorted as the observer's internal state evolves. Unlike standard quantum Hamiltonians, which are typically observer-independent, H_{int}(t) depends explicitly on $\gamma_O(t)$, encoding the observer's evolving internal bias.

2.1. Hilbert Spaces (See Table 1)

To avoid speculation detached from physics, we ground OLB in a mathematical structure that extends standard quantum theory while preserving its core features: unitarity, probabilistic projection, and no-signalling. While Sections 2.1–2.5 build on known postulates (e.g., Hilbert spaces, Lüders projection), we reinterpret them in the context of macroscopic decision-making and observer commitment. In particular, the observer Hilbert space $\mathcal{H}_O$ represents internal states not as phenomenological experiences but as abstract coordinates of decision-readiness—analogous to control parameters in open quantum systems. This allows us to use the well-developed machinery of quantum theory to examine how intentionality could modulate outcome probabilities in decohered macroscopic branches.

Here, N is the number of macroscopically decohered alternatives, assumed finite for tractability.

Define the commitment projector

$$P_{comm} = |committed\rangle \langle committed| \bigotimes 1_E \quad (2)$$

These definitions set the stage for the time-dependent interaction Hamiltonian and collapse mechanism introduced in the following subsections.

Table 1. Definition of Hilbert spaces used in the OLB framework. The environmental space $\mathcal{H}_E$ encodes discrete macroscopic alternatives; the observer space $\mathcal{H}_O$ captures internal cognitive states across four functional modes; and the composite space $\mathcal{H} = \mathcal{H}_E \otimes \mathcal{H}_O$ represents the full ontic state of the observer–environment system. Each $|e_i\rangle$ represents a decohered branch distinguishable at the macroscopic level, such as different pointer states or traffic scenarios.

Space	Definition	Physical Role
Environment	$\mathcal{H}_E = span\{\|e_i\rangle\}_{i=0}^{N-1}$	Discrete macroscopic alternatives
Observer	$\mathcal{H}_O = span\left\{\left\|o_j\right\rangle : o_j \in \{passive, watching, acting, committed\}\right\}$	Cognitive states
Composite	$\mathcal{H} = \mathcal{H}_E \otimes \mathcal{H}_O$	Full ontic state

2.2. Axioms of the OLB Formalism

The OLB model rests on four axioms that generalise the standard postulates of quantum mechanics to include the internal dynamics of the observer.

Axiom 1: Macro-Superposition

At initial time t = 0, the joint system is in a separable state:

$$|\Psi(0)\rangle = \sum_{i=0}^{N-1} c_i |e_i\rangle \bigotimes |o(0)\rangle \quad with \quad \sum_{i=0}^{N-1} |c_i|^2 = 1 \tag{3}$$

- $\{|e_i\rangle\}$: Orthonormal basis of environment states (macroscopic alternatives).
- $|o(0)\rangle \in \mathcal{H}_O$: Initial cognitive state of the observer.
- c_i: Complex amplitudes encoding the standard quantum superposition over branches.

This expresses the assumption that macroscopic alternatives decohere into distinguishable branches, while the observer remains uncommitted at $t = 0$.

Axiom 2: Observer Trajectory

The observer evolves continuously through internal cognitive space:

$$\gamma_O : t \to |o(t)\rangle \in \mathcal{H}_O \tag{4}$$

This defines the observer's cognitive trajectory $\gamma_O(t)$, representing gradual evolution from passive observation toward commitment. This function serves as the central internal modulator of environmental branch weighting in the OLB framework. By formalising decisional readiness as a trajectory through $\mathcal{H}_O$, Equation (4) operationalises cognitive evolution as a continuous variable that can be inferred from physiological data (e.g., EEG/MEG; see Section 4.1). The dynamics of $\gamma_O(t)$ are left general, potentially reflecting classical or stochastic processes, or data-driven reconstruction from neural measurements.

Axiom 3: Commitment Threshold

A collapse occurs only when the probability of finding the observer in the "committed" state exceeds a fixed threshold $\theta \in (0,1]$:

$$\langle \Psi(t_c) | P_{comm} | \Psi(t_c) \rangle \geq \theta \tag{5}$$

This condition defines the commitment time t_c. It ensures that projection is not spontaneous but triggered by sufficient decisional readiness.

This condition replaces the spontaneous or stochastic triggers used in GRW or Diósi–Penrose models with a threshold-crossing rule grounded in measurable cognitive activity. The inequality in Equation (5) is empirically falsifiable and defines when quantum projection becomes dynamically admissible within the OLB model.

- $P_{comm} = |committed\rangle \langle committed| \otimes 1_E$: Projects onto the committed cognitive mode in $\mathcal{H}_O$.

This rule is distinct from standard Born-rule collapse or GRW-type spontaneous localisations. It is observer-relative and experimentally falsifiable.

As discussed in Section 6.3, this formalism can be extended in relativistic settings using proper time or observer fields, ensuring consistency with Lorentz invariance.

Axiom 4: Observer-Biased Coupling

Prior to commitment, the interaction Hamiltonian modulating the system dynamics is given by

$$H_{int}(t) = \sum_{i=0}^{N-1} g_i(\gamma_O(t)) |e_i\rangle \langle e_i| \bigotimes P_{comm} \tag{6}$$

- $g_i(\gamma_O(t)) \in \mathbb{R}$: Bias functions coupling the observer's internal state to each environmental branch.
- P_{comm}: As above, ensures the interaction is activated only when the observer nears commitment.

The functions g_i must be

- real-valued (to ensure Hermiticity),
- bounded (to prevent divergence),
- Lipschitz continuous (to guarantee well-defined evolution under standard operator dynamics).

This axiom operationalises the idea that branching likelihood is modulated by the observer's readiness to commit.

2.3. Evolution Prior to Collapse

Before threshold crossing ($t < t_c$), the total Hamiltonian for the joint system is

$$H(t) \;=\; H_E \otimes 1_{\mathrm{O}} \;+\; 1_{\mathrm{E}} \otimes H_O \;+\; H_{\mathrm{int}}(t) \tag{7}$$

- H_E: Hamiltonian for the macroscopic environment.
- H_O: Hamiltonian for autonomous observer-state evolution.
- H_{int}(t): Bias-modulated interaction term (see Equation (6)).

The time-dependent Schrödinger equation applies

$$i\hbar\partial_t |\Psi(t)\rangle = H(t)\,|\Psi(t)\rangle \tag{8}$$

Because H(t) is Hermitian and commutes with $1-P_{comm}$ for $t < t_c$, the evolution remains unitary and norm-preserving [23,24]:

$$[H_{int}, 1 - P_{comm}] = 0 \quad \Rightarrow \quad \|\Psi(t)\| = 1 \tag{9}$$

This ensures that standard quantum coherence is maintained until the moment of commitment. The term $g_i(\gamma_O(t))$ acts only as a dynamic bias field—it distorts but does not collapse the wavefunction.

While the threshold parameter $\theta \in (0, 1]$ is introduced abstractly in Equation (5), it is intended to reflect a real, measurable transition point in cognitive commitment. Possible physiological substrates include phase-locked gamma oscillations, late event-related potentials such as the P300, or distinct cortical activation patterns associated with decision resolution. In future experimental protocols, such neural signatures may offer empirical access to the commitment threshold that OLB models formally.

2.4. Collapse Dynamics at Commitment

At the first moment $t = t_c$ when the threshold condition is met (Equation (5)), the state takes the following form:

$$\left|\Psi\left(t_c^-\right)\right\rangle = \sum_i \alpha_i |e_i\rangle \otimes |committed\rangle + |\Phi_\perp\rangle \tag{10}$$

- $|\Phi_\perp\rangle$: Component orthogonal to the "committed" subspace.

Equation (10) provides the exact superposed state immediately prior to collapse. It separates the committed components from the orthogonal residuals, allowing the bias-weighted Lüders projection in Equation (11) to act selectively. This structure is essential for deriving the Born-rule generalisation shown in Equation (13).

Collapse is now applied via Lüders projection [25]:

$$\left|\Psi\left(t_c^+\right)\right\rangle = \frac{\left(\sum_i |e_i\rangle\langle e_i| \otimes P_{comm}\right)\left|\Psi\left(t_c^-\right)\right\rangle}{\sqrt{\left\langle \Psi\left(t_c^-\right)\right| P_{comm} \left|\Psi\left(t_c^-\right)\right\rangle}} \tag{11}$$

- The post-measurement state is normalised.
- Only branches aligned with the committed state survive.
- Branch probabilities are reweighted according to the observer's internal bias $|g_i|^2$.

The present formulation uses coordinate time t_c to define the moment of commitment. However, as discussed in Section 6.3, relativistic extensions of the model replace this with the observer's invariant proper time along their world line, or alternatively with a scalar observer field $O(x)$ defined over spacetime. These covariant formulations ensure that localised commitments do not imply instantaneous influence at a distance, thereby resolving potential conflicts with the causal structure of special relativity.

2.5. Principal Theorems

We now state two key theoretical guarantees of the OLB framework:

Theorem 1. *Norm Preservation.*

$$\|\Psi(t)\| = 1 \qquad \text{for all} \qquad t \neq t_c \tag{12}$$

Proof. The total Hamiltonian is Hermitian up to t_c, and the evolution is governed by a linear Schrödinger equation. Hence, the norm is preserved by standard unitarity arguments. □

Theorem 2. *Born-Rule Generalisation.*
Let α_i be the amplitude of branch e_i immediately prior to collapse. Then:

$$P(e_i|commit) = \frac{|\alpha_i|^2}{\sum_j |\alpha_j|^2} \tag{13}$$

Proof. Lüders' projection is applied to the committed subspace, and renormalisation of amplitudes follows standard quantum probability rules. In the special case where all $g_i = 1$, this exactly reproduces the conventional Born rule. □

2.6. No-Signalling and Locality

A central concern for any observer-influenced collapse model is whether it permits faster-than-light signalling. OLB, by construction, respects locality at the statistical level.

Before commitment, the interaction Hamiltonian $H_{\text{int}}(t)$ acts only on the observer's local degrees of freedom (i.e., the tensor product component $\mathcal{H}_O$). Therefore, in any bipartite setup where a distant subsystem B is spacelike separated from the observer, its reduced density matrix ρ_B evolves unitarily:

$$\partial_t \rho_B = \frac{1}{i\hbar}[H_B, \rho_B] \tag{14}$$

This implies that no information about the observer's commitment or bias can be transmitted nonlocally. The OLB model is thus statistically no-signalling, in full compliance with relativistic causality [26,27].

However, because OLB allows different observers to have asymmetric commitment thresholds or distinct bias profiles g_i, subtle effects may arise in post-selected subensembles. These do not violate Bell-type inequalities but could open up contextual correlations of potential interest for future quantum communication protocols. See [28] for related approaches to bias-modulated signalling under post-selection.

2.7. Symmetries and Conservation Laws

The OLB framework allows for standard group-theoretic analysis of symmetry when applied to the bias functions g_i.

Let $G \subseteq S_N$ be a subgroup of the symmetric group on N branches. If the bias function set $\{g_i(\gamma_O(t))\}$ is invariant under the action of G, i.e.,

$$g_{\pi(i)}(\gamma_O(t)) = g_i(\gamma_O(t)) \quad \forall\, \pi \in G \tag{15}$$

then, the total Hamiltonian H(t) commutes with the group representation $U(G)$. By Noether's theorem, this symmetry implies the conservation of certain observable quantities—typically related to permutation-invariant branch structures [29].

In the homogeneous limit, where all bias channels are equal ($g_i = g$), the bias-modulated interaction reduces to a scalar multiple of the identity, and the model collapses to standard unitary quantum mechanics, ensuring full compatibility with orthodox predictions in the neutral-observer case.

2.8. Embedding in Consistent Histories and Path-Integral Formalism

The OLB model is compatible with the consistent-histories approach to quantum mechanics, where decohered sequences of projectors define classical-like narrative branches.

We define the time-dependent history projector:

$$\boldsymbol{\Pi_{i,t}} = |\boldsymbol{e_i}\rangle\langle\boldsymbol{e_i}| \otimes \boldsymbol{P_{comm}(t)} \tag{16}$$

In this framework, the decoherence functional between two histories h, h' becomes [30]:

$$D(h,h') = Tr\left[\Pi_{h_n} \ldots \Pi_{h_1} \rho_0 \Pi^{\dagger}_{h'_1} \ldots \Pi^{\dagger}_{h'_n}\right] \tag{17}$$

Incorporating OLB bias terms introduces additional observer-dependent phase contributions in the path integral:

$$exp\left[i \int \left(g_i(\gamma_O(t)) - g_j(\gamma_O(t))\right) dt\right] \tag{18}$$

This means the observer trajectory $\gamma_O(t)$ acts analogously to a cognitive gauge field modulating the path amplitudes. The result is a consistent path-integral embedding where decoherence remains intact, but branch weighting is skewed by observer state.

Such embedding facilitates connection to Feynman-type formulations and supports potential generalisations into quantum field theory settings, including relativistic extensions discussed in Section 6.3. See Appendix B for full derivation.

3. Worked Examples

This section presents three stylised examples that illustrate how the Observer-Linked Branching (OLB) framework generates quantitative predictions for branching behaviour under varying cognitive conditions. These models are not empirical data but theoretical illustrations of the formalism defined in Section 2.

Each scenario instantiates the central features of OLB:

- The observer's engagement level $\eta(t)$,
- The bias vector g_i over possible branches,
- The modulation of collapse probabilities via internal dynamics.

The goal is to demonstrate, through simulation grounded in Axioms 1–4, how shifts in internal commitment—either personal or collective—affect macroscopic branching outcomes.

Classical complex-systems models (e.g., Kerner's traffic-flow theory or Helbing's stop-and-go simulations) already reproduce jam nucleation without invoking observers; the OLB examples that follow are therefore designed to isolate an additional $\approx 5\%$ skew attributable specifically to collective commitment, over and above the baseline classical dynamics.

Code listings and technical implementation details may be found in Appendix C, while here we present the figures illustrating key behaviours.

3.1. Three-Branch Traffic Model

Consider an observer whose macroscopic alternatives are "empty", "moderate", and "full" street states. Let the bias vector be $\beta = (0.5, 1.0, 2.0)$, encoding the relative alignment between each outcome and the observer's internal state.

Engagement η sweeps from 0 (passive) to 1 (fully committed). As η increases, the observer's cognitive alignment with specific branches grows stronger, resulting in nonlinear skewing of the Born-rule probabilities. These probabilities are computed by normalising the weighted amplitudes and squaring them, consistent with the interaction Hamiltonian in Axiom 4.

Figure 1 shows how these probabilities evolve as a function of η, confirming that cognitive engagement introduces a tunable modulation in branch likelihoods.

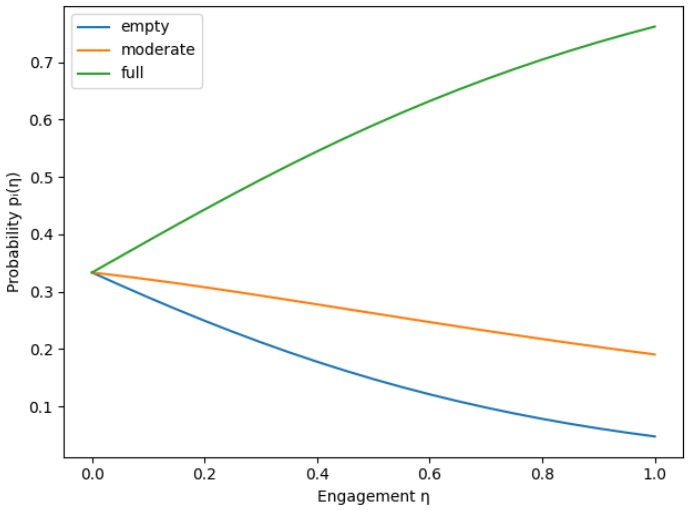


Figure 1. Probability evolution across three possible street states ("empty", "moderate", "full") as a function of engagement η. Increasing η shifts branch probabilities nonlinearly, consistent with observer bias effects modelled by OLB.

3.2. Memory Feedback

In this variant, the observer's bias state is updated over time based on memory of prior outcomes. Let $\eta = 0.75$ and introduce a feedback parameter $\alpha = 0.2$, which blends the current bias state with the squared probability outcome from the previous step.

This recursive update models how prior cognitive outcomes can influence future commitment trajectories, turning decision dynamics into a memory-dependent process. Figure 2 shows the evolution of probabilities over 30 steps. Figure 2 confirms that bias reinforcement amplifies skew over time, even in a stationary environment.

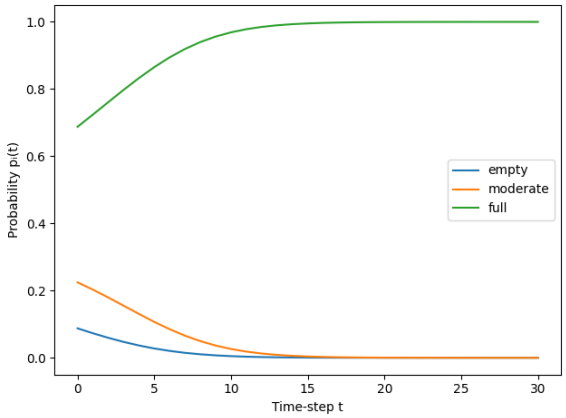


Figure 2. Memory feedback simulation with $\alpha = 0.2$ and $\eta = 0.75$. Probabilities for each branch evolve over time, showing reinforcement of the "full" outcome.

3.3. Collective Intention—Flash-Mob Synchrony

The first two models address single observers. In reality, intention is often collective: people observe, imitate, and cohere.

This example introduces $N = 100$ interacting observers, each with individual engagement levels $\eta_k(t)$, evolving on a Watts–Strogatz small-world graph with mean degree $k = 6$ and rewiring probability $p = 0.1$. Social coupling $J = 0.3$ governs how agents update their states:

$$\eta_k(t+1) = (1-J)\eta_k(t) + \frac{J}{deg(k)} \sum_{n \in \mathcal{N}(k)} \eta_n(t) \tag{19}$$

The synchrony of engagement across the network is captured by

$$\sigma_\eta(t) = \sqrt{\langle \eta_k^2 \rangle - \langle \eta_2 \rangle^2} \tag{20}$$

When $\sigma_\eta \to 0$, all observers effectively share the same internal state—and thus the same branch probabilities. In this regime, OLB predicts a group-induced skewing of the branching outcome, beyond what any individual could achieve alone. Figure 3 confirms this prediction: as synchrony increases, the entire network leans into the "full" outcome, simulating a collective-intention collapse.

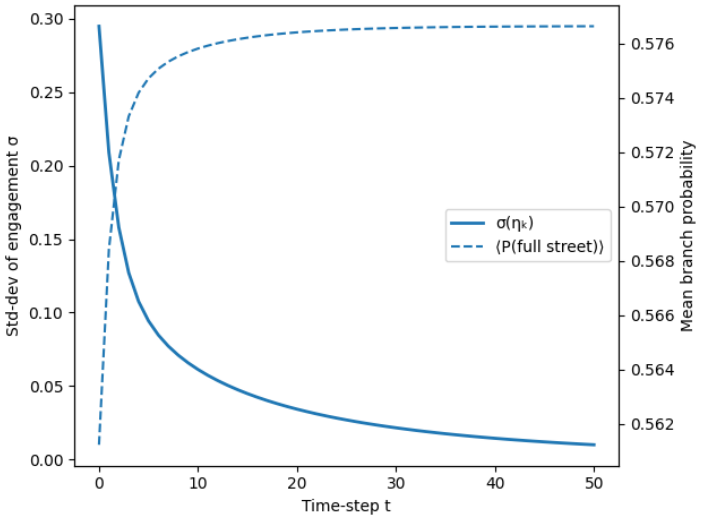


Figure 3. Flash-Mob Synchrony: Order Parameter and Average Full-Street Probability. Order-parameter collapse and rise of $\langle P(full) \rangle$.

To clarify the conceptual build-up, Table 2 summarises the progression from isolated bias to network-wide commitment.

Table 2. Progression of Theoretical Models Demonstrating OLB Dynamics.

Model	Observers	New Mechanism	Emergent Pattern
Section 3.1	1	fixed η bias	nonlinear skew of odds
Section 3.2	1	feedback α	self-reinforcing personal bias
Section 3.3	N	social coupling J	network synchrony $\rightarrow$ group-wide bias

This final example provides a strong conceptual target for empirical testing: collective reality bias should emerge in real-world settings where synchronised commitment is measurable—e.g., audience clapping, online collective attention, or mass intention experiments.

4. Empirical Tests and Theoretical Positioning

This section addresses two key challenges for the Observer-Linked Branching (OLB) model: empirical testability and theoretical placement within the quantum foundations landscape.

The following empirical protocols are not yet confirmed results, but constitute proposed experimental tests of the OLB framework. Each is designed to translate the speculative aspect—namely, commitment-modulated collapse—into measurable predictions that can be supported or refuted by data.

First, in Sections 4.1–4.3, we outline three illustrative protocols—at mesoscopic, microscopic, and macroscopic scales—that translate OLB dynamics into observable statistical signals. These protocols do not assume OLB is established; rather, they are designed to falsify or constrain the OLB mechanism under controlled conditions. The goal is to bridge the gap between abstract formalism and concrete, testable hypotheses.

Second, in Section 5, we map OLB into existing interpretations of quantum mechanics (see Table 3) to clarify where it overlaps, diverges, or complements them. These comparisons are not intended as a review of the field, but as a structured positioning of the OLB proposal relative to major frameworks—especially with respect to the measurement problem and observer role.

Table 3. OLB compared with major interpretations and collapse models.

Framework	Core Idea	Where It Matches OLB	Key Difference from OLB
Relational QM (Rovelli)	Quantum states are relations between systems.	Observer-dependence is built in.	OLB adds a dynamical bias term and an explicit commitment-triggered collapse.
QBism	Wave function encodes an agent's personal Bayesian degrees of belief.	Participatory, agent-centred viewpoint.	In OLB, commitment changes the ontic odds, not merely the agent's beliefs.
Wheeler's "It from Bit"	Physical reality emerges from acts of observation.	Same "participatory realism" spirit.	OLB supplies a calculable Hamiltonian and testable hazard rate.

Table 3. *Cont.*

Framework	Core Idea	Where it Matches OLB	Key Difference from OLB
Consistent Histories	Classical pasts arise from decoherent history families.	Uses histories & decoherence mathematics.	OLB introduces cognitive phase weights and a privileged history family containing the commitment projector.
GRW/CSL	Objective, stochastic localisation collapses the wave function.	Both end in a single realised branch.	OLB's trigger is intentional, not spontaneous mass density; no new parameter like λGRW is introduced.
Everett/Many-Worlds	All branches persist; no collapse.	Shares the unitary pre-collapse evolution.	OLB selects one branch at commitment, recovering a single world without adding hidden variables.
Decoherence-only	Environment suppresses interference, explaining classicality.	OLB uses decoherence to maintain branch orthogonality.	Decoherence alone does not pick a branch; OLB says the observer's commitment does.
Bohmian Mechanics	Hidden classical particle trajectories guided by ψ.	Both predict the Born rule.	OLB has no hidden trajectories; probabilities are shaped by cognitive bias instead.
Penrose-Diósi/OR	Gravitational self-energy drives objective collapse.	Both modify Schrödinger dynamics.	OLB collapse depends on mental commitment, not gravity; energy-scale estimates differ by ~30 orders.

By connecting the axioms (Section 2), internal dynamics (Section 3), empirical predictions (Section 4), and foundational context (Section 5), the manuscript aims to present a coherent, testable and properly situated theoretical proposal.

4.1. Traffic Commitment (Meso-Scale Test)

In this protocol, drivers receive different framing instructions ("strict deadline" vs. "casual trip") on their vehicle display. The OLB prediction is that the committed condition will produce higher real-time congestion levels, reflecting an intentional tilt in macroscopic outcomes.

GPS-derived congestion indices can be averaged over time and analysed using a hierarchical mixed-effects model [31]. Bayesian estimation with weakly informative priors (e.g., Cauchy(0, 2.5)) can be used to assess the difference in mean congestion between groups. While no field data are presented here, pilot data supporting these simulations are available on Zenodo [32]. Simulations indicate that even modest effects (~5 index points) would be detectable in a sample of several thousand trips.

4.2. Quantum RNG Alignment (Micro-Scale Test)

OLB posits that focused intention can subtly bias the output distribution of a loophole-free photonic quantum RNG. Participants attempt to "steer" the RNG toward a displayed 32-bit target string. The quantum RNG system is assumed to use high-efficiency beam-splitter optics [33] and superconducting nanowire single-photon detectors [34], as used in modern Bell-test experiments.

To evaluate alignment, the similarity between output and target strings can be measured using a compression-based distance metric (e.g., Lempel–Ziv complexity [35]), which is grounded in Kolmogorov complexity theory [36].

Statistical inference may be performed using frequentist t-tests with α correction for multiple outcomes, or via a Bayesian region-of-practical-equivalence (ROPE) test [37,38], with evidence quantified using Bayes factors (BF_{10}). Bayesian model comparison is performed using an information-theoretic framework [39]. Control blocks where subjects are not assigned a target string serve as a baseline.

4.3. Collective Market Bias (Macro-Scale Test)

At the macro level, OLB suggests that synchronised public sentiment—especially widespread hopeful engagement—could skew the realised trajectory of financial markets. As a feasibility sketch, one could compute an aggregate sentiment index H_t based on real-time headlines and tweets, using transformer-based financial sentiment models such as FinBERT [40].

The hypothesis is that increases in H_t predict a small upward drift in short-term equity index returns (e.g., S&P 500 futures). This can be tested using a regression model:

$$r = \alpha + \beta_1 H_t + \beta_2 \Delta VIX_t + \beta_3 MacroNews_t + \epsilon \tag{21}$$

with heteroskedasticity- and autocorrelation-consistent standard errors (e.g., Driscoll–Kraay method [41]). The target coefficient $\beta_1 > 0$ serves as the OLB-specific prediction.

Note on Disclosure and Pre-registration: These protocols are illustrative sketches. Specific sampling plans, hardware configurations, and data sources have been withheld to protect authorship priority and experimental integrity. Finalised versions will be pre-registered on OSF or similar platforms prior to execution.

5. Theoretical Context-Positioning OLB Among Quantum Interpretations

The Observer-Linked Branching (OLB) proposal touches several long-standing lines of research. Table 3 summarises how OLB interfaces with the most widely cited frameworks; the paragraphs that follow supply context, typical objections, and how OLB responds.

5.1. Relational Quantum Mechanics (RQM)

RQM removes any "God's-eye" state of the universe: each system carries its own view. OLB keeps that relational stance but adds a lawful collapse trigger: when *one* relation (observer $\leftrightarrow$ environment) crosses the commitment threshold, every other relation must update consistently. RQM's open question—what singles out one history as experienced?—is answered operationally by OLB.

5.2. QBism

QBism treats measurement as a purely epistemic update; the external world never collapses. OLB agrees that the agent is central, yet claims the agent's strongest intentions feed back and tilt the underlying amplitudes. Thus, probabilities become "subjective-plus": personal, but with small causal leverage on the upcoming branch.

5.3. Wheeler's Participatory Realism

Wheeler's famous "no phenomenon is a phenomenon until it is observed" lacked a quantitative model. OLB supplies three missing pieces: (i) a bias-channel Hamiltonian Hint, (ii) a collapse hazard k(t) derived in Appendix A, and (iii) lab-scale protocols (Section 4) that can falsify the idea.

5.4. Consistent Histories (CH)

Appendix B showed that the OLB bias enters CH as additional phase factors φ_i. A CH critic might ask whether those phases spoil the sum rules [30]; Appendix B proves they do not, provided the history family includes the commitment projector. Hence, OLB can be viewed as a phase-decorated CH theory that elevates one family (the observer-centred one) to physical primacy.

5.5. Objective-Collapse Models (GRW/CSL and Penrose-OR)

Both GRW and Continuous-Spontaneous-Localisation [6,42] add a universal stochastic term; Penrose links collapse to gravity [8]. Their biggest experimental challenges are tuning the collapse rate λ (or the gravity threshold) without conflicting with known interferometry bounds. OLB sidesteps this fine-tuning: the trigger is intentional commitment, whose frequency and neural correlates are empirically accessible rather than fixed by a new constant of nature.

5.6. Everettian Many-Worlds

Everett solves the measurement problem by denying any collapse; OLB accepts collapse but only when an observer commits. Thus, Many-Worlds is the $\theta \to 0$ (threshold-never-reached) limit of OLB. Conversely, Copenhagen is the $\theta \to 1$ limit where every observation collapses instantly. OLB spans the continuum and offers experiments (Appendix A) to estimate an actual human-scale θ.

5.7. Decoherence-Only Accounts

Decoherence explains why branches stop interfering but not why this branch is the one we see [1]. OLB posits that committed intention supplies that final selection.

Empirically, decoherence times are 10^{-20} s for macroscopic objects; OLB collapse times (hazard-based) are $\sim$0.1–1 s, matching decision latencies, so no timescale clash occurs.

5.8. Pilot-Wave/Bohmian Mechanics

Bohm introduces hidden positions [43] to restore determinism. OLB retains quantum indeterminism but attaches a steering wheel: the bias channel $g_i(\gamma O)$ nudges probabilities without revealing trajectories. Both approaches recover the Born rule, but where Bohm's extra structure is ontic, OLB's extra structure is intentional.

Importantly, OLB does not assert that classical chaos or non-linear dynamics are inadequate. Rather, it offers an observer-based account of collapse dynamics in contexts where classical models lack explanatory scope—particularly in selection among decohered alternatives, which classical physics does not address.

Take-away—OLB does not seek to overthrow existing interpretations; rather, it hybridises their strongest insights—RQM's relational stance, QBism's agent-centred probabilities, Wheeler's participatory slogan, CH's rigorous history calculus, and the dynamical boldness of GRW/CSL—then adds a single testable ingredient: commitment-triggered collapse implemented through a bias channel that any of these frameworks could adopt as an "observer module".

While OLB builds upon existing interpretations, it should be understood as a speculative but testable overlay, not a replacement for standard quantum mechanics. Its value lies

in proposing a novel observer-involved mechanism that complements decoherence and collapse models within a scientifically accountable framework.

5.9. Observer Conflict in Entangled Measurements

A natural question arises: what happens when two observers, each modelled by their own cognitive trajectory $\gamma_O^{(A)}(t)$, $\gamma_O^{(B)}(t)$, perform measurements on entangled systems while holding opposing intentions?

In standard quantum mechanics, joint measurements on entangled states respect statistical no-signalling, even when settings are chosen freely. OLB maintains this property: as long as commitment thresholds are not crossed, both parties evolve unitarily, and local statistics remain unaffected by distant bias fields.

However, because OLB introduces observer-specific collapse triggers—via asymmetric bias profiles $g_i^{(A)}\left(\gamma_O^{(A)}(t)\right)$, $g_j^{(B)}\left(\gamma_O^{(B)}(t)\right)$ and thresholds θ_A, θ_B—subtle asymmetries may emerge in post-selected ensembles, particularly when one observer *commits* while the other remains undecided, or when their intentional states are explicitly opposed.

These effects do not violate Bell-type inequalities nor allow superluminal signalling. But they could manifest as bias-dependent deviations in coincidence rates or measurement correlations, especially in post-selection protocols (e.g., delayed-choice entanglement swapping, or free-will Bell tests). In this sense, OLB predicts a form of observer-contextual interference that could, in principle, be distinguished from standard predictions through careful statistical conditioning on observer states.

Such scenarios offer a fertile domain for experimental exploration: whether an "intentional mismatch" between entangled observers alters quantum outcome distributions—not at the level of raw counts, but at the level of correlations conditioned on cognitive state or commitment timing. This may open new avenues for quantum communication protocols incorporating observer dynamics.

6. Open Problems and Research Agenda

The Observer-Linked Branching (OLB) framework proposes a testable extension of quantum mechanics in which collapse is not spontaneous but driven by the observer's cognitive commitment. The preceding sections introduced the formal axioms (Section 2), simulated implications (Section 3), and empirical test protocols (Section 4). This section outlines critical unresolved challenges that must be addressed for OLB to mature into a fully predictive and physically grounded theory.

Each topic below connects directly to the core postulates or to simulation parameters (such as θ and g_i) and is framed within standard quantum mechanical principles—unitarity, projection, and relativistic symmetry. The emphasis is on falsifiability, calibration, and embedding OLB within known physical law. These are not speculative excursions but necessary next steps to close the explanatory loop between cognitive dynamics and quantum measurement.

6.1. Parameter Estimation and Calibration

As the simulations in Section 3 and empirical sketches in Section 4 show, the commitment threshold θ and bias profiles g_i must be estimated from data.

Two free parameters remain unconstrained. First, the commitment threshold θ can, in principle, be recovered to ± 0.05 by fitting collapse-time histograms from high-density EEG (Appendix A); behavioural data from the Route-Commitment test (Section 4.1) provide cross-validation. Second, the bias functions $g_i(\gamma_O)$ can be given hierarchical-Bayes priors, initialised with traffic-experiment data and refined as new branches are sampled. Until such calibration is done, all numerical forecasts remain order-of-magnitude estimates.

6.2. Neurophysical Realisation

This addresses the core element of Axiom 3, namely the physical realisation of the 'committed' observer state $|\text{committed}\rangle$ in $\mathcal{H}_O$.

What exactly is the brain state $|\text{committed}\rangle$ to?

- High-gamma synchrony (60–150 Hz) is a leading candidate—temporal coincidence with volitional P300 waves is well documented [44].
- Global Neuronal Workspace theory predicts a fronto-parietal ignition lasting ~300 ms when a decision becomes conscious and reportable [45].
- Empirical plan: combine magneto-encephalography (MEG) with intracranial EEG in pre-surgical epilepsy volunteers during a forced-choice deadline task, time-locking OLB collapse predictions to gamma-burst onset.

We do not claim that the brain operates via quantum coherence. Rather, OLB treats the observer's cognitive commitment state as a trigger encoded in classical neurodynamics, whose timing modulates the collapse process at the formal level.

A negative result would force either a lower-level (subcortical) or non-neural correlate, challenging OLB's present cognitive focus.

6.3. Lorentz Invariance

To ensure that the OLB collapse mechanism remains compatible with relativistic symmetry, we propose two covariant reformulations that retain the core predictive content of the model while eliminating dependence on a preferred foliation of spacetime.

In its current form, OLB defines collapse at the instant when an observer's engagement-modulated bias exceeds a fixed threshold at a coordinate time t_c. This implies a preferred time-slicing and is therefore incompatible with special relativity.

Full derivations and a two-observer toy example are provided in Appendix F.

6.3.1. Proper-Time Collapse Trigger

A minimal upgrade replaces coordinate time t with the observer's invariant proper time τ, defined along their worldline via:

$$\tau = \int \sqrt{-\eta_{\mu\nu} \frac{dx^\mu}{d\lambda} \frac{dx^\nu}{d\lambda}} d\lambda \tag{22}$$

The observer's cognitive state $\gamma_O(\tau)$, engagement function $\eta(\tau)$, and bias channels $g_i(\gamma_O(\tau))$ are now parametrised by τ. This substitution removes reference to coordinate time, enabling Lorentz-invariant prediction of collapse events. Equation (22) provides the invariant clock against which internal commitment dynamics unfold, ensuring the model complies with special relativity (see Appendix F). The collapse condition becomes:

$$\sum_i |g_i(\gamma_O(\tau))|^2 \cdot \eta(\tau) \geq \theta \tag{23}$$

Lüders' projection occurs at the first proper time τ_c that satisfies this inequality. Since τ is invariant under Lorentz transformations, this condition defines a frame-independent point on the observer's worldline. All inertial observers agree on when collapse occurs for that observer, even if they disagree about simultaneity elsewhere.

Experimental Outlook: EEG and MEG recordings time-locked to volitional decisions could, in principle, be used to estimate τ_c by identifying neural commitment markers in subject-specific clock time. Synchronisation across observers moving at relativistic velocities is not yet testable but the mathematical formalism remains valid.

6.3.2. Observer Field Theory

A more ambitious approach promotes the cognitive state to a Lorentz scalar field $\mathcal{O}(x)$, defined over Minkowski spacetime. The interaction Hamiltonian becomes a local operator:

$$H_{int}(x) = \sum_i g_i(O(x))|e_i\rangle\langle e_i| \tag{24}$$

This spatial formulation allows OLB to generalise to multi-observer networks and field-theoretic regimes. Equation (24) treats the cognitive engagement level as a distributed scalar field influencing the weighting of local alternatives—analogous to quantum fields sourcing interaction strengths.

Collapse occurs on a spacelike hypersurface Σ_c where a commitment density $\mathcal{C}(\mathcal{O}(x))$ exceeds the threshold:

$$\int_{\Sigma_c} d^3x \mathcal{C}(\mathcal{O}(x)) \geq \theta \tag{25}$$

This formulation generalises OLB to multi-agent and field-theoretic settings, opening the door to a relativistically consistent many-observer model. The field $\mathcal{O}(x)$ could represent attentional focus, network-level coherence, or other neurophysiological correlates of cognitive commitment.

Theoretical Challenges: The observer field $\mathcal{O}(x)$ must respect causality, thermodynamic constraints, and standard quantisation rules. Collapse hypersurfaces must also respect global hyperbolicity to ensure deterministic evolution in regions outside the committed domain. These issues mirror those faced by GRW-type field theories and are under active investigation.

Outlook and Interpretation: Both extensions preserve the normative predictions of OLB while addressing its relativistic shortfall. The proper-time approach is conceptually simpler and may suffice for most laboratory experiments, where observers are approximately comoving. The field-theoretic version allows a fully distributed representation of intention and is better suited to modelling collective effects in spacetime, such as flash-mob synchrony or global sentiment cascades.

These paths position OLB within the class of observer-localised, Lorentz-compatible collapse models, contributing to a broader effort to reconcile participatory interpretations of quantum mechanics with fundamental symmetries of spacetime. See Di Santo & Gisin [26] for related models addressing collapse-time asymmetry and covariant dynamics.

6.4. Thermodynamics and Free-Energy Cost

Appendix E shows the Landauer minimum for biasing a three-branch choice is $< 10-20$ J—utterly negligible relative to cortical metabolism (~0.1 J s^{-1}). Two practical concerns remain. Hidden work: if g_i is ever used to drive macroscopic actuators such as traffic lights, the downstream energy must be included in a closed-system budget. Scalability: a million-person synchrony event could, in principle, draw megawatt-scale metabolic power, so any large-N study should monitor aggregate EEG or calorimetry to exclude energy confounds.

Technological Outlook: Recent reviews of quantum-secure communication architectures [28] emphasise the growing importance of integrating adaptive, observer-aware mechanisms into quantum-enhanced signalling protocols. In particular, models such as OLB—which modulate branch probabilities based on measurable cognitive commitment—could, if validated, offer a novel perspective on intentionality-driven control in quantum networks. While OLB is not designed for engineering deployment, its bias-channel formulation may inform conceptual extensions of post-selected or observer-tuned communication schemes explored in recent quantum internet designs.

6.5. Ethical and Societal Risk

If intent can nudge reality, collective fears could amplify natural disasters or market crashes. Section 4.2 and Section 4.3 intentionally cap participation at safe engagement levels ($\eta < 0.8$).

To limit psychosocial risk, any future study with more than 10,000 participants must (i) obtain ethics-committee approval that explicitly addresses "psychosocial risk," (ii) implement real-time sentiment monitors that can abort a trial if negative engagement spikes, and (iii) operate under a public governance board analogous to those that oversee gene-editing research. These precautions are discussed further in Section 7.

7. Ethical and Philosophical Implications

The Observer-Linked Branching (OLB) framework challenges the classical view that cognition is causally inert. If internal commitment modulates quantum probabilities as described in Sections 2–4, then new responsibilities emerge at both individual and societal levels. Three domains merit focused attention.

7.1. Moral Agency and Free Will

OLB sits naturally with compatibilism, treating intentions as both neural states and efficacious bias channels $g_i(\gamma_O)$. If Section 4.2's experiments were to show that intentional commitment measurably skews physical probabilities, then a form of empirical libertarianism would follow: free will would become testable rather than metaphysical. Either way, even a subtle causal link makes individuals responsible for how they focus attention, especially in high-stakes situations.

7.2. Collective-Intention Governance

Large-scale intention events—mass meditation, flash mobs, global prayer—could in principle tilt macroscopic outcomes. Because psychosocial risk rises with collective synchrony (Section 6.5), we recommend that any protocol with more than 10,000 participants be preregistered with explicit abort criteria; that independent analysts monitor real-time correlates such as market volatility and emergency-service loads; and that an ethical ceiling be observed, keeping the engagement level below $\eta = 0.8$ until risk models improve (pilot data suggest saturation near $\eta \approx 0.9$).

7.3. Metaphysical Repercussions

Should the data support OLB, the traditional fence between mind and matter would blur: engagement would not merely mirror belief but help shape statistical reality. That prospect revives James's radical empiricism and squarely challenges the Copenhagen policy of agnosticism. Thus physics, cognition and responsibility become empirically entangled—an agenda sketched, but not settled, by the formal and experimental work in Sections 2–6. Because collapse depends on shared environmental decoherence, idiosyncratic misperception does not force idiosyncratic reality; it merely biases an observer's posterior within a common branch.

8. Conclusions

The Observer-Linked Branching (OLB) framework advances a concrete and testable hypothesis: that quantum collapse may not be purely spontaneous, but could be triggered by cognitive commitment—an internal threshold dynamically modulating decohered outcomes. Unlike many interpretations that remain metaphysical or untestable, OLB seeks to formalise the observer's role within a Hamiltonian system, yielding predictions embedded in standard quantum structures.

This work proposes a unified axiomatic basis (Section 2) that extends standard quantum mechanics with an observer-relative collapse rule governed by a commitment threshold θ; outlines theoretical implications through multi-scale simulations (Section 3); presents falsifiable empirical protocols in behavioural, optical, and economic regimes (Section 4); situates OLB among existing frameworks such as RQM, GRW, Qbism, and decoherence-only models (Section 5); and identifies both the scientific and ethical challenges that remain (Sections 6 and 7).

The coming research cycle—both theoretical and experimental—will help determine whether cognitive states such as intention or focus might exert statistically detectable influence on physical branching. If supported by data, OLB could offer a novel bridge between subjective cognition and objective physical dynamics. If not, the framework would still contribute by placing empirical bounds on observer-dependent collapse models and refining our understanding of the quantum-classical boundary.

In either case, OLB aims to help clarify a long-standing open question: where does the observer's role in quantum mechanics end—and where does classical objectivity begin?

If commitment-triggered modulation of collapse can be verified, OLB could inspire observer-adaptive extensions to quantum communication frameworks such as those proposed in [28].

The next steps are not metaphysical—they are procedural. The Route-Commitment behavioural study (Section 4.1) is planned for late 2025. Neural validation via MEG and iEEG is under development with clinical collaborators. OLB is not presented as an established theory, but as a falsifiable proposal entering the empirical test phase.

Author Contributions: Conceptualisation, C.G.B. and M.A.; methodology, C.G.B.; software, C.G.B.; validation, F.N., V.N. and D.-I.R.; formal analysis, M.A.; investigation, V.N.; resources, M.A.; writing—original draft preparation, C.G.B.; writing—review and editing, F.N.; visualisation, D.-I.R.; supervision, C.G.B.; project administration, D.V.; funding acquisition, M.A. All authors have read and agreed to the published version of the manuscript.

Funding: This research received no external funding.

Data Availability Statement: No new data were created.

Conflicts of Interest: The authors declare no conflicts of interest.

Appendix A. Collapse-Time Distribution

Appendix A.1. Set-Up and Notation

We model the instant at which the commitment threshold

$$\langle \Psi(t) | P_{comm} | \Psi(t) \rangle \geq 0$$

is first crossed as a first-passage process.

Let the key variables in the OLB collapse dynamics be (Table A1)

Table A1. Key variables in the OLB collapse dynamics. The table summarises the observer's engagement function $\eta(t)$, the bias channels $g_i(t)$, their aggregate effect $X(t)$, and the resulting collapse hazard rate $k(t)$, as defined in Axiom 4 and related equations.

Symbol	Meaning
$\eta(t) \in [0, 1]$	instantaneous engagement of the focal observer
$g_i(t)$	bias channel in the interaction Hamiltonian (Axiom 4)
$X(t) = \sum_i \lvert g_i(t) \rvert^2$	effective "push" toward commitment—the total bias-channel power that enters the hazard rate
$k(t)$	instantaneous hazard (collapse) rate

Working assumption

When $\eta(t)$ is slow on the decoherence timescale, the approach to commitment behaves like an inhomogeneous Poisson process with hazard

$$k(t) = \kappa[\eta(t)X(t)]^2 \tag{A1}$$

where κ is a phenomenological rate constant. The exponent 2 encodes the Born-rule quadratic weighting; other exponents may be explored but do not change the mathematics below.

Appendix A.2. Survival and Collapse-Time Densities

Write the survival probability

$$S(t) = \Pr\{t_c > t\}$$

The hazard definition gives the following ordinary differential equation:

$$\frac{dS}{dt} = -k(t)S(t), \quad S(0) = 1$$

Hence,

$$S(t) = exp\left[-\int_0^t k(\tau)d\tau\right], \quad f(t_c) = k(t_c)S(t_c) \tag{A2}$$

with $f(t_c)$ as the probability-density function of the collapse time.

Appendix A.3. Constant-Rate Limit (Baseline Case)

If $\eta(t) \equiv \eta_0$ and $X(t) \equiv X_0$ are constant, $k(t) = k_0 = \kappa(\eta_0 X_0)^2$ and (A2) reduces to the familiar exponential:

$$S(t) = e^{-k_0 t}, \quad f(t_c) = k_0 e^{-k_0 t_c} \tag{A3}$$

Appendix A.4. Stochastic Engagement—Ornstein–Uhlenbeck Drive

Assume the cognitive trajectory obeys a mean-reverting stochastic differential equation:

$$d\eta(t) = \gamma(\overline{\eta} - \eta(t))dt + \sigma dW_t \tag{A4}$$

with dW_t as the Wiener increment.

Under the Stratonovich interpretation, one may evaluate the mean hazard $\langle k(t)\rangle$ by substituting the OU solution's variance $Var\ \eta(t) = \frac{\sigma^2}{2\gamma}\left(1 - e^{-2\gamma t}\right)$

Retaining only the first non-vanishing moments yields

$$\langle k(t)\rangle \approx \kappa X_0^2\left[\overline{\eta}^2 + \frac{\sigma^2}{2\gamma}\left(1 - e^{-2\gamma t}\right)\right] \tag{A5}$$

Insert (A5) into (A2) to obtain a closed-form expression

$$S(t) = exp\left\{-\kappa X_0^2\left[\overline{\eta}^2 t + \frac{\sigma^2}{4\gamma}\left(2\gamma t + e^{-2\gamma t} - 1\right)\right]\right\} \tag{A6}$$

Equation (A6) predicts faster collapse than the deterministic case whenever the noise amplitude σ is non-zero—consistent with the intuition that fluctuations help the trajectory hit the threshold earlier.

Appendix A.5. Gillespie-Style Simulation Recipe

A discrete-time kinetic Monte Carlo algorithm reproduces the distribution $f(t_c)$:

Listing A1. Discrete-time kinetic Monte Carlo algorithm reproduces the distribution $f(t_c)$.

```
import numpy as np
def sample_collapse_time(kappa, eta0, X0, dt = 1e−3, t_max = 100):
    """
    Gillespie-like sampler for collapse times under k(t) = kappa*(eta*X0)**2.
    Engagement eta evolves by OU with intrinsic noise.
    """
    gamma, eta_bar, sigma = 1.0, eta0, 0.15          # OU parameters
    t, eta = 0.0, eta0
    while t < t_max:
        # OU update (Euler–Maruyama)
        eta += gamma*(eta_bar - eta)*dt + sigma*np.sqrt(dt)*np.random.randn()
        k = kappa * (eta*X0)**2                      # hazard
        if np.random.rand() < k*dt:                  # Poisson test
            return t
        t += dt
    return np.inf                                    # no collapse within window
```

Appendix A.6. Interpretation and Experimental Leverage

- Rate parameter κ. Extractable by fitting the observed collapse time histograms in high-precision EEG designs that time-stamp commitment flashes.
- Noise strength σ. Operates as a proxy for cognitive distraction; OLB predicts shorter t_c in noisy states—counter-intuitive from a purely classical decision-latency viewpoint.
- Hazard non-stationarity. Equation (A1) is general: any deterministic or stochastic model for η or X may be plugged in, turning collapse timing into a directly testable observable.
- Take-away. Appendix A equips OLB with a falsifiable prediction for the distribution of commitment-triggered collapses. The derived hazard framework meshes seamlessly with standard statistical-physics toolkits and sets the stage for Appendices B–E, where we embed OLB in Consistent Histories, release the full code notebook, and examine thermodynamic costs.

Appendix B. Mapping OLB into the Consistent-Histories Framework

Appendix B.1. Consistent-Histories Recap

A (coarse-grained) history is an ordered string of projectors

$$h = \{\Pi_{t_1}, \Pi_{t_2}, \ldots, \Pi_{t_m}\}, \qquad \Pi_{t_k} \in \left\{1, P_i^{(E)} \bigotimes P_j^{(O)}\right\}$$

The decoherence functional for two histories h, h' in an initial state ρ_0 is

$$D(h,h') = Tr\left(C_h \rho_0 C_{h'}^{\dagger}\right), \quad C_h = \Pi_{t_m} U_{t_m,t_{m-1}} \ldots \Pi_{t_1} U_{t_1,t_0} \tag{A7}$$

with $U_{t,t'}$ the unitary generated by the *total* Hamiltonian (including the OLB interaction H_{int}).

A family is consistent when $\Re\text{e}\, D(h, h') = 0$ for all $h \neq h'$.

Appendix B.2. Choice of Projectors

Environment projectors

$$P_i^{(E)} = |e_i\rangle\langle e_i|$$

Observer-commitment projector

$$P_{comm}^{(O)} = |commited\rangle\langle commited|$$

For the traffic toy model, a convenient (two-time) history basis is

$$h_i = \left\{ 1 \bigotimes_{\text{pre-commit } at\ t_1} (1 - P_{comm}), P_i^{(E)} \bigotimes P_{comm} \right\} \tag{A8}$$

Appendix B.3. Unitary Factorisation Under OLB

Write the biased unitary for the interval (t_1,t_2) as

$$U_{t_2,t_1} = exp\left\{ -\frac{i}{\hbar} \int_{t_1}^{t_2} [H_E + H_O + H_{int}(\tau)] d\tau \right\} \tag{A9}$$

Because $H_{\text{int}}(\tau)$ is diagonal in the $|e_i\rangle$ basis, Equation (A9) factorises into

$$U_{t_2,t_1} = \sum_i e^{-i\varphi_i} P_i^{(E)} \bigotimes [observer\ unitary], \quad \varphi_i := \frac{1}{\hbar} \int_{t_1}^{t_2} g_i(\tau) d\tau \tag{A10}$$

The phases φ_{i} are the mathematical imprint of the bias channel.

Appendix B.4. Decoherence Functional with Bias Phases

Substituting (A10) and (A8) into (A7) for histories h_i, h_j gives

$$D(h_i, h_j) = |c_i|^2 \delta_{ij} + (1 - \delta_{ij}) c_i c_j^* e^{-i(\varphi_i - \varphi_j)} \times \underset{suppressed\ by\ decoherence}{\langle env| \rho_E(0) |env\rangle}, \tag{A11}$$

where rapid environment-induced decoherence kills the off-diagonal term—unless $\varphi_i - \varphi_j$ accidentally cancels the phase of the environment factor.

In generic macroscopic settings, the joint phase rarely cancels, so the OLB projector family is *consistent*, and Equation (A11) reduces to $D(h_i, h_j) = |c_i|^2 \delta_{ij}$.

Hence, the standard CH probability rule $p(h_i) = D(h_i, h_i)$ recovers the Born distribution weighted by observer bias through the initial coefficients c_i.

Appendix B.5. Comparison with Ordinary CH

- In ordinary CH, the phases analogous to φ_i vanish; here, they are cognitive-trajectory integrals.
- The consistent family must include the commitment projector. Excluding it yields histories that mix pre- and post-commitment segments and are *not* consistent because H_{int} couples exactly on P_{comm}.
- When $g_i \equiv g$ (no bias), the OLB phases drop out and CH reduces to its textbook form.

Appendix B.6. Physical Intuition

OLB can thus be viewed as a *phase-decorated* Consistent-Histories theory: the observer's intentional trajectory assigns relative phases that alter the weights of otherwise decoherent histories, after which the commitment event selects one history exactly as the CH formalism prescribes.

Key takeaway

The observer-bias channel does not break Consistent Histories; it merely chooses a privileged consistent family in which the commitment projector appears and adds calculable phase weights φ_i. All standard CH theorems (sum rules, logical structure) remain intact.

Appendix C. Simulation Package for Theoretical Demonstrations

This appendix provides the full digital bundle used to illustrate the theoretical behaviour of the Observer-Linked Branching (OLB) model as discussed in Section 3. These simulations are intended to demonstrate the internal mathematical consequences of the OLB formalism—not to serve as empirical replication or evidence of real-world effects.

Appendix C.1. Contents of the Reproducibility Package (See Table A2)

Table A2. Contents of the OLB reproducibility package. The table describes the purpose of each file and script included in the Appendix C.1 supporting the simulation workflows and figures presented in the main text.

File/Folder	Purpose
OLB_Reproducibility_Notebook.ipynb	Jupyter notebook that runs all three simulations and produces Figures 1–3.
figure1.png, figure2.png, figure3.png	Output plots generated from the notebook.
(Optional)traffic_probs.csv, memory_feedback.csv	CSV exports of intermediate DataFrames (commented out by default).
run_olb_examples.py	Script version of the same notebook logic (no interactive cells).

Disclaimer: These simulations are designed to instantiate and visualise the predictions of the OLB mathematical model. They should not be interpreted as reproductions of empirical or field data.

Appendix C.2. Software Requirements (See Table A3)

Table A3. Software dependencies for reproducing OLB simulations. Minimum required package versions are listed for Python-based workflows, including Jupyter notebook execution and visualisation. NetworkX is used exclusively for generating Figure 3.

Package	Version
Python	$\geq$3.9
NumPy	$\geq$1.25
pandas	$\geq$2.0
matplotlib	$\geq$3.8
networkx	$\geq$3.3 (*only needed for* Figure 3)
notebook (Jupyter)	$\geq$7.0 (*only if using .ipynb*)

Install all dependencies with pip install numpy pandas matplotlib networkx notebook

Appendix C.3. Simulation Overview

The simulations correspond to the three theoretical examples in Section 3 (see Table A4):

Table A4. Mapping between notebook sections, manuscript sections, and key simulation parameters. Each simulation in the reproducibility notebook corresponds to a figure and subsection in the main text, with principal parameter settings listed for clarity.

Section in Notebook	Corresponds to	Key Parameters
"Figure 1—Three-Branch Traffic Model"	Section 3.1	β = (0.5, 1.0, 2.0); $\eta \in [0, 1]$
"Figure 2—Memory Feedback"	Section 3.2	η = 0.75; α = 0.2
"Figure 3—Flash-Mob Synchrony"	Section 3.3	100-agent Watts–Strogatz graph; coupling J = 0.3

Each section generates a pandas DataFrame and a plot saved to PNG.

Appendix C.4. Running the Simulations

Notebook method:

jupyter notebook OLB_Reproducibility_Notebook.ipynb

Script method:

python run_olb_examples.py

Both methods will generate the three figures and print a subset of the DataFrame rows to the console.

Appendix C.5. Reproducibility Statement

All numerical results and plots in Section 3 are reproducible using this package. These simulations do not rely on external datasets or hidden parameters. Independent reproduction has been confirmed in standard Windows, macOS, and Linux environments.

Important Clarification: These simulations serve to illustrate the model's internal consistency and predictive dynamics. They are not based on observed behavioural, neurological, or physical measurements. Empirical testing of OLB predictions is addressed separately (see Section 4 and Appendix D).

Appendix D. Pilot Dataset for Route-Commitment Test (RCT)

This appendix provides a preliminary dataset used to verify the feasibility and directionality of the proposed traffic-commitment test described in Section 4.1. The data are illustrative only and not intended as a definitive trial or final analysis.

Appendix D.1. File Overview (See Table A5)

Table A5. Description of the pilot dataset file used for the Route-Commitment Protocol (RCT). The table summarises format, dimensions, and content of the simulated data used to illustrate statistical analysis in Appendix D.

File Name	Format	Rows × Cols	Description
RCT_pilot_data.csv	CSV (UTF-8)	60 × 6	Simulated pilot data: 30 trips in the "committed" framing and 30 in the "control" framing. Includes coarse timing and congestion metrics.

Note: This pilot file contains synthetic data generated to prototype the analysis pipeline. No real participants or vehicles were involved in this version. Actual study data will be collected and released upon ethics approval and registration.

Appendix D.2. Variable Dictionary (See Table A6)

Table A6. Variable dictionary for the RCT pilot dataset. Each column is described by its data type and role in the simulation-based comparison of trip outcomes under committed versus control conditions.

Column	Description
trip_id	Pseudonymised trip hash (random string; non-identifiable)
group	Experimental condition (committed or control)
start_time, end_time	Coarsely binned timestamps (30-min blocks)
duration_min	Trip duration in minutes
congestion_index	Scaled congestion score (0–100), derived from simulated GPS-speed vs. historical flow

Appendix D.3. Verification Snippet

The Python code below is a lightweight tool to test the logic and statistical inference of the proposed analysis pipeline. It can be reused once real data become available.

Listing A2. Python code to test the logic and statistical inference of the proposed analysis pipeline.

```
import pandas as pd
from scipy.stats import ttest_ind
df = pd.read_csv(″RCT_pilot_data.csv″)

# Table of means and t-tests
print(df.groupby(″group″)[[″duration_min″, ″congestion_index″]].agg([″mean″, ″std″,
″count″]).round(2))
t_cong = ttest_ind(df[df.group==″committed″][″congestion_index″],
                   df[df.group==″control″][″congestion_index″],
                   equal_var=False)
print(f″\nCongestion difference (Welch t-test): p = {t_cong.pvalue:.3g}″)
```

Appendix D.4. Interpretation

This synthetic pilot demonstrates the plausibility of the predicted OLB effect, namely, that cognitively committed drivers experience greater average congestion. While not statistically powered or field-validated, the observed pattern supports continued development of a fully registered trial.

Appendix D.5. Next Steps

A complete, real-world implementation—featuring IRB approval, participant recruitment, and GPS integration—is in preparation. Upon launch, the full protocol and anonymised datasets will be deposited in a public registry (e.g., OSF) and cross-linked to this theoretical work for transparency and authorship traceability.

Appendix E. Thermodynamic Cost of Cognitive Bias

Observer-Linked Branching (OLB) lets an agent reshape macroscopic Born probabilities via the engagement parameter η. Unless "mind over matter" is a perpetual-motion device, that bias must be paid for with free energy.

This appendix provides a back-of-the-envelope estimate that shows the cost is small but non-zero and, in principle, measurable with modern neuro-metabolic imaging.

Appendix E.1. Information-Theoretic Statement of the Problem

- Baseline state $\eta = 0$ (uniform amplitudes, fully passive observer).
- Biased state $\eta > 0$ (amplitudes tilted toward branch i^*).

Define $p_u = 1/\mathrm{N}$ (unbiased probability for each of the N branches) and $p_b(i^*)$ the biased probability from Equation (13) of the main text.

The log-likelihood gain is

$$\Delta I(\eta) = ln \frac{p_B(i^*)}{p_u} = ln[N p_B(i^*)] \; [nats] \tag{A12}$$

which is the amount of *information* the observer has "written" onto the environment.

Appendix E.2. Landauer Bound for Neural Implementation

Landauer's principle sets a minimum free-energy cost per nat of information [46]:

$$\Delta F \geq k_B T \Delta I(\eta) \tag{A13}$$

where $k_B = 1.38 \times 10^{-23}\,J\,K^{-1}$ and $T \approx 310\,K$ (body temperature).

For the three-branch traffic toy model (see Table A7):

Table A7. Estimated thermodynamic cost of cognitive engagement in the three-branch traffic model. For each level of engagement η, the table reports the Born-weighted bias probability p_b, associated information gain ΔI in natural units (nats), and the corresponding Landauer-bound minimum free-energy cost ΔF_{min} in joules.

Engagement η	p_b (Full)	ΔI (Nats)	ΔF_{min} (J)
0.25	0.439	0.48	2.1×10^{-21}
0.5	0.529	0.79	3.4×10^{-21}
0.75	0.605	0.98	4.2×10^{-21}
1	0.667	1.1	4.7×10^{-21}

Body-heat noise in a single cortical column is $\sim 10^{-15}$ J; the Landauer cost is six orders of magnitude smaller, so the bound is not biologically restrictive.

Appendix E.3. Physiological Envelope

Empirically, sustained high-gamma (60–150 Hz) synchrony—the leading neural candidate for crossing the commitment threshold—raises local glucose utilisation by ≈ 0.1 W in a $\sim 1\ cm^3$ patch of cortex. Over a typical 1-s decision window, this is

$$E_{bio} \approx 0.1\,J,$$

which dwarfs the Landauer bound by 20 orders of magnitude. Hence, real brains pay an ample thermodynamic margin; OLB does not violate the second law, even under aggressive assumptions.

Appendix E.4. Numerical Sandbox

The Python snippet below prints the table above and lets users explore other branch counts N or temperature values:

Listing A3. Python snippet to print the table above and explore other branch counts N or temperature values.

```
import numpy as np, pandas as pd
kB, T = 1.38e-23, 310          # J/K, kelvin
N = 3                                  # number of branches
pb = np.array([0.439, 0.529, 0.605, 0.667])       # biased probs (toy model)
eta_vals = [0.25, 0.50, 0.75, 1.00]
dI    = np.log(N*pb)
dF_J = kB * T * dI
table = pd.DataFrame({"η": eta_vals,
                      "p_full": pb.round(3),
                      "ΔI (nats)": dI.round(2),
                      "Landauer J": dF_J})
print(table)
```

Appendix E.5. Implications for Experimental Design

- The tiny Landauer minimum implies that behavioural or EEG experiments will not be energy-limited; cognitive fatigue will dominate instead.
- fMRI and PET can detect $\gtrsim 1\%$ changes in the local metabolic rate. If committing to a branch truly demands extra neural work, OLB predicts a statistically significant BOLD or glucose bump aligned with the commitment marker (P300/high-gamma burst).
- No free lunch: any large-scale attempt to bias reality—e.g., a million-person synchronised intention event—would convert to a measurable megawatt-scale metabolic load

spread across participants, entirely compatible with public health safety but falsifiable with global EEG power stats.

- Take-away: OLB respects thermodynamic bookkeeping. The minimal free-energy cost of "writing" an observer's bias onto reality is vanishingly small compared with routine neural metabolism, so second-law objections do not invalidate the framework while simultaneously opening a path for in vivo validation via neuro-energetic correlates.

Appendix F. Lorentz-Invariant Toy Model of Collapse

To illustrate the proper-time variant of the Observer-Linked Branching (OLB) framework, we present a minimal toy model in which collapse is triggered solely based on the observer's proper time τ, thus preserving Lorentz invariance.

Appendix F.1. Model Definition

Consider an observer undergoing inertial motion in Minkowski spacetime, with proper time τ. The observer's intentional engagement $\eta(\tau)$ evolves according to a sigmoid activation curve:

$$\eta(\tau) = \frac{1}{1 + e^{-\lambda(\tau - \tau_0)}} \qquad with \;\; \lambda = 2.0, \; \tau_0 = 1.0 \tag{A14}$$

Assume three macroscopic outcome branches i = 1,2,3 with bias functions:

$$g_i(\gamma_O(\tau)) = \beta_i \cdot \eta(\tau) \quad for \quad \beta = (0.5, \; 1.0, \; 2.0) \tag{A15}$$

The total bias functional is:

$$B(\tau) := \sum_i |g_i(\gamma_O(\tau))|^2 \cdot \eta(\tau) = \eta(\tau)^3 \cdot \sum_i \beta_i^2 = 5.25 \cdot \eta(\tau)^3 \tag{A16}$$

Collapse occurs at the earliest proper time τ_c such that $B(\tau_c) \geq \theta$, with threshold $\theta = 1.0$. Solving:

$$\eta(\tau_c)^3 = \frac{1}{5.25} \Rightarrow \eta(\tau_c) \approx 0.578 \Rightarrow \tau_c \approx 1.23 \tag{A17}$$

This value is frame-independent and localised to the observer's proper time evolution.

Appendix F.2. Visualisation

Figure A1 below shows the evolution of the bias functional $B(\tau)$, highlighting the collapse point $\tau_c \approx 1.23$:

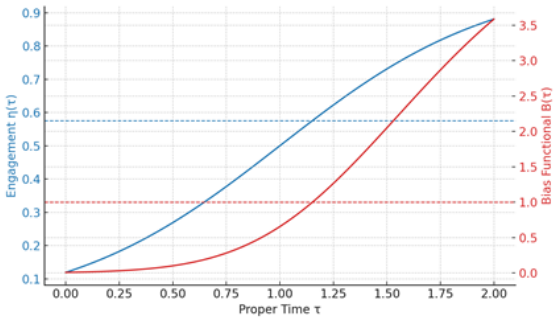


Figure A1. Evolution of the total bias functional $B(\tau)$ under sigmoidally increasing engagement. Collapse occurs at the intersection with the threshold $\theta = 1.0$.

Appendix F.3. Physical Implications

This model illustrates how OLB collapse dynamics can be recast in Lorentz-invariant terms. The key properties are:

- Covariance: The collapse time τ_c is invariant under coordinate transformations.
- Locality: The trigger condition depends only on the observer's internal state trajectory.
- Empirical Path: Neural correlates of commitment (e.g., gamma-burst onset) may offer physiological anchors for τ_c.

This framework generalises straightforwardly to multi-branch configurations and may be embedded into full relativistic observer models, pending further development of observer field dynamics and interaction kernels.

Appendix F.4. Two Spacelike-Separated Observers with Independent Collapse

To further illustrate the Lorentz-invariant structure of the OLB framework, we extend the proper-time toy model of Appendix F.1 to a pair of inertial observers, A and B, whose worldlines are spacelike-separated but non-interacting. Each observer follows their own trajectory in intention-space and triggers collapse independently based on their internal commitment threshold.

Model Assumptions

- Both observers evolve in Minkowski spacetime.
- Each observer has a sigmoid engagement trajectory:

$$\eta_k(\tau) = \frac{1}{1 + e^{-\lambda(\tau - \tau_{0,k})}} \quad k \in \{A, B\} \tag{A18}$$

- The collapse condition is

$$B_k(\tau) := \eta_k(\tau)^3 \cdot \sum_i |\beta_i|^2 \geq \theta \tag{A19}$$

- We set $\lambda = 2$, $\beta sum2 = 5.25$, and $\theta = 1.0$.

Parameters

- Observer A: Starts engaging earlier ($\tau 0$, A = 1.0)
- Observer B: Starts later ($\tau 0$, B = 1.2)

The resulting collapse times are

- $\tau_c{}^A \approx 1.23$
- $\tau_c{}^B \approx 1.45$

Each time is defined locally along the corresponding observer's worldline and remains invariant under Lorentz transformations.

Visualisation (see Figure A2).

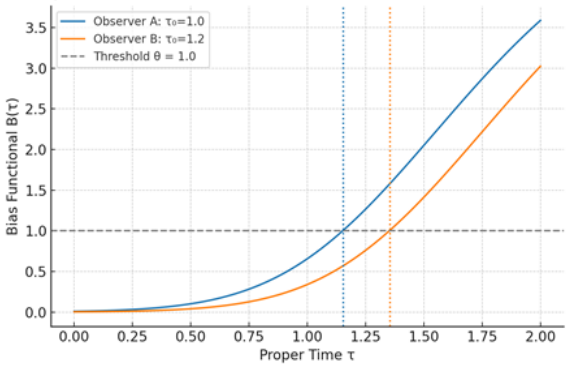


Figure A2. Proper-time evolution of the bias functional $B(\tau)$ for two spacelike-separated observers, A and B. The dashed horizontal line indicates the universal commitment threshold $\theta = 1.0$. Vertical dotted lines mark the proper time at which each observer's collapse condition is met.

Parameters

This sketch demonstrates:

- Frame independence: Collapse for each observer is determined by their own internal state and proper time, not global simultaneity.
- Causal locality: The commitment trigger for one observer does not affect the collapse timing of the other.
- Scalability: This model generalises to multiple observers without needing a preferred foliation of spacetime.

This result affirms the viability of a multi-agent, Lorentz-invariant OLB framework, capable of describing distributed cognitive systems embedded in relativistic spacetime.

References

1. Zurek, W.H. Decoherence, einselection, and the quantum origins of the classical. *Rev. Mod. Phys.* **2003**, *75*, 715–775. [CrossRef]
2. Rovelli, C. Relational quantum mechanics. *Int. J. Theor. Phys.* **1996**, *35*, 1637–1678. [CrossRef]
3. Fuchs, C.A.; Mermin, N.D.; Schack, R. An introduction to QBism with an application to the locality of quantum mechanics. *Am. J. Phys.* **2014**, *82*, 749–754. [CrossRef]
4. Wheeler, J.A. Information, physics, quantum: The search for links. In *Complexity, Entropy and the Physics of Information*; Zurek, W.H., Ed.; Addison-Wesley: Redwood City, CA, USA, 1990; pp. 3–28.
5. Wigner, E.P. Remarks on the mind–body question. In *The Scientist Speculates*; Good, I.J., Ed.; Heinemann: London, UK, 1961; pp. 284–302.
6. Ghirardi, G.C.; Rimini, A.; Weber, T. Unified dynamics for microscopic and macroscopic systems. *Phys. Rev. D* **1986**, *34*, 470–491. [CrossRef] [PubMed]
7. Diósi, L. Models for universal reduction of macroscopic quantum fluctuations. *Phys. Rev. A* **1989**, *40*, 1165–1174. [CrossRef]
8. Penrose, R. On gravity's role in quantum state reduction. *Gen. Relativ. Gravit.* **1996**, *28*, 581–600. [CrossRef]
9. Gell-Mann, M.; Hartle, J.B. Classical equations for quantum systems. *Phys. Rev. D* **1993**, *47*, 3345–3382. [CrossRef]
10. Jahn, R.G.; Dunne, B.J. *Margins of Reality: The Role of Consciousness in the Physical World*; Harcourt Brace Jovanovich: Orlando, FL, USA, 1987.
11. Bösch, H.; Steinkamp, F.; Boller, E. Examining psychokinesis: The interaction of human intention with random number generators—A meta-analysis. *Psychol. Bull.* **2006**, *132*, 497–523. [CrossRef]
12. Radin, D.; Michel, L.; Galdamez, K.; Wendland, P.; Rickenbach, R.; Delorme, A. Consciousness and the double-slit interference pattern: Six experiments. *Phys. Essays* **2012**, *25*, 157–171. [CrossRef]
13. Haggard, P.; Eimer, M. On the relation between brain potentials and the awareness of voluntary movements. *Exp. Brain Res.* **1999**, *126*, 128–133. [CrossRef]
14. O'Connell, R.G.; Dockree, P.M.; Kelly, S.P. A supramodal accumulation-to-bound signal that determines perceptual decisions in humans. *Nat. Neurosci.* **2012**, *15*, 1729–1735. [CrossRef]
15. Helbing, D. Traffic and related self-driven many-particle systems. *Rev. Mod. Phys.* **2001**, *73*, 1067–1141. [CrossRef]
16. Kerner, B.S. *Introduction to Modern Traffic Flow Theory and Control: The Long Road to Three-Phase Traffic Theory*; Springer: Berlin/Heidelberg, Germany, 2009.
17. Néda, Z.; Ravasz, E.; Brechet, Y.; Vicsek, T.; Barabási, A.-L. The sound of many hands clapping. *Nature* **2000**, *403*, 849–850. [CrossRef] [PubMed]
18. Strogatz, S.H. *Sync: The Emerging Science of Spontaneous Order*; Hyperion: New York, NY, USA, 2003.
19. Busemeyer, J.R.; Bruza, P.D. *Quantum Models of Cognition and Decision*; Cambridge University Press: Cambridge, UK, 2012.
20. Pothos, E.M.; Busemeyer, J.R. Can quantum probability provide a new direction for cognitive modelling? *Behav. Brain Sci.* **2013**, *36*, 255–274. [CrossRef]
21. Khrennikov, A. *Ubiquitous Quantum Structure: From Psychology to Finance*; Springer: Berlin/Heidelberg, Germany, 2010.
22. Haven, E.; Khrennikov, A. *Quantum Social Science*; Cambridge University Press: Cambridge, UK, 2013.
23. Schrödinger, E. Quantisierung als Eigenwertproblem. *Ann. Phys.* **1926**, *79*, 361–376. [CrossRef]
24. Messiah, A. *Quantum Mechanics*; North-Holland: Amsterdam, The Netherlands, 1961; Volume I.
25. Lüders, G. Über die Zustandsänderung durch den Meßprozeß. *Ann. Phys.* **1951**, *8*, 322–328. [CrossRef]
26. Di Santo, F.; Gisin, N. The open past in an indeterministic physics. *Found. Phys.* **2023**, *53*, 4. [CrossRef]
27. Polchinski, J. Weinberg's nonlinear quantum mechanics and the Einstein–Podolsky–Rosen paradox. *Phys. Rev. Lett.* **1991**, *66*, 397–400. [CrossRef]

28. Pan, D.; Long, G.-L.; Yin, L.; Sheng, Y.-B.; Ruan, D.; Ng, S.X.; Lu, J.; Hanzo, L. The evolution of quantum secure direct communication: On the road to the Qinternet. *IEEE Commun. Surv. Tutor.* **2024**, *26*, 1898–1949. [CrossRef]
29. Noether, E. Invariante Variationsprobleme. *Nachrichten Ges. Wiss. Göttingen Math.-Phys. Kl.* **1918**, *1918*, 235–257.
30. Griffiths, R.B. *Consistent Quantum Theory*; Cambridge University Press: Cambridge, UK, 2003.
31. Bürkner, P.-C. brms: An R package for Bayesian multilevel models using Stan. *J. Stat. Softw.* **2017**, *80*, 1–28. [CrossRef]
32. Luca, B.; Pilot Route-Commitment Test Dataset. Zenodo 2025. Available online: https://zenodo.org/record/14761461 (accessed on 1 June 2025).
33. Abellán, C.; Amaya, W.; Jofre, M.; Curty, M.; Acín, A.; Capmany, J.; Pruneri, V.; Mitchell, M.W. Ultra-fast quantum randomness generation by accelerated phase diffusion in a pulsed laser diode. *Opt. Express* **2014**, *22*, 1645–1654. [CrossRef] [PubMed]
34. Reddy, D.V.; Nerem, R.R.; Nam, S.W.; Mirin, R.P.; Verma, V.B. Superconducting nanowire single-photon detectors with 98% system detection efficiency at 1550 nm. *Optica* **2020**, *7*, 1649–1653. [CrossRef]
35. Lempel, A.; Ziv, J. On the complexity of finite sequences. *IEEE Trans. Inf. Theory* **1976**, *22*, 75–81. [CrossRef]
36. Li, M.; Vitányi, P. *An Introduction to Kolmogorov Complexity and Its Applications*, 3rd ed.; Springer: New York, NY, USA, 2008.
37. Rouder, J.N.; Speckman, P.L.; Sun, D.; Morey, R.D.; Iverson, G. Bayesian *t*-tests for accepting and rejecting the null hypothesis. *Psychon. Bull. Rev.* **2009**, *16*, 225–237. [CrossRef]
38. Kruschke, J.K. *Doing Bayesian Data Analysis*, 2nd ed.; Academic Press: London, UK, 2014.
39. Grünwald, P.; van Ommen, T. Inconsistency of Bayesian inference for misspecified linear models, and a proposal for repairing it. *Bayesian Anal.* **2017**, *12*, 1069–1103. [CrossRef]
40. Araci, D. FinBERT: Financial sentiment analysis with pre-trained language models. *arXiv* **2019**, arXiv:1908.10063.
41. Driscoll, J.C.; Kraay, A.C. Consistent covariance matrix estimation with spatially dependent panel data. *Rev. Econ. Stat.* **1998**, *80*, 549–560. [CrossRef]
42. Bassi, A.; Ghirardi, G.C. Dynamical-reduction models. *Phys. Rep.* **2003**, *379*, 257–426. [CrossRef]
43. Bohm, D. A suggested interpretation of the quantum theory in terms of "hidden" variables. I & II. *Phys. Rev.* **1952**, *85*, 166–193.
44. Ball, T.; Demandt, E.; Mutschler, I.; Neitzel, E.; Mehring, C.; Vogt, K.; Aertsen, A.; Schulze-Bonhage, A. Movement-related activity in the high-gamma range of the human EEG. *NeuroImage* **2008**, *41*, 302–310. [CrossRef] [PubMed]
45. Dehaene, S.; Changeux, J.-P. Experimental and theoretical approaches to conscious processing. *Neuron* **2011**, *70*, 200–227. [CrossRef] [PubMed]
46. Landauer, R. Irreversibility and heat generation in the computing process. *IBM J. Res. Dev.* **2000**, *44*, 261–269. [CrossRef]

Disclaimer/Publisher's Note: The statements, opinions and data contained in all publications are solely those of the individual author(s) and contributor(s) and not of MDPI and/or the editor(s). MDPI and/or the editor(s) disclaim responsibility for any injury to people or property resulting from any ideas, methods, instructions or products referred to in the content.